Mandibular bone is protected against microarchitectural alterations and bone marrow adipose conversion in ovariectomized rats

Xavier Coutel, Jérôme Delattre, Pierre Marchandise, Guillaume Falgayrac, Hélène Béhal, Greet Kerckhofs, Guillaume Penel, Cécile Olejnik

Mandibular bone is protected against microarchitectural alterations and bone marrow adipose conversion in ovariectomized rats

Xavier COUTEL*[1], Jérôme DELATTRE[1], Pierre MARCHANDISE[1], Guillaume FALGAYRAC[1], Hélène BEHAL[2], Greet KERCKHOFS[3,4,5,6], Guillaume PENEL[1] , Cécile OLEJNIK [1],

1. Univ.Lille, Univ. Littoral Côte d'Opale, CHU Lille, EA 4490 - PMOI, F-59000 Lille, France
2. Univ. Lille, CHU Lille, EA 2694 - Santé publique: épidémiologie et qualité des soins, Unité de Méthodologie et Biostatistiques, F-59000 Lille, France
3. Biomechanics lab, Institute of Mechanics, Materials, and Civil Engineering, UCLouvain, Louvain-la-Neuve, Belgium
4. Institute of Experimental and Clinical Research, UCLouvain, Woluwe, Belgium
5. Department Materials Engineering, KU Leuven, Leuven, Belgium
6. Prometheus, Division of Skeletal Tissue Engineering, KU Leuven, Leuven, Belgium

Corresponding author e-mail: xavier.coutel@univ-lille.fr

ABSTRACT

Osteoporosis is a disease that leads to a loss of bone mass and to alterations in the bone microarchitecture that occur in a site-specific manner; however it remains controversial in the jaw. The involvement of bone marrow adipose tissue (BMAT) in the bone metabolism has been suggested in several physiopathological contexts, such as in aging and osteoporosis. To test whether the BMAT content is related to mandibular bone loss, this study aimed to investigate the potential correlations between the trabecular bone microarchitecture on one hand and BMAT content and its spatial distribution in relation to bone surface on the other hand during aging and ovariectomy (OVX) during a long-term follow-up in a mature rat model.

No age-related microarchitectural or BMAT changes were observed in the mandible. The OVX-induced bone loss was three-fold lower in the mandible than in the tibia and was observed only in the alveolar bone (not in the condyle). We also report a delayed increase in the mandibular BMAT content that remained 4-6-fold lower compared to tibia. This low BMAT content in the mandible was located at a distance from the trabecular bone surface (only 5% in contact with the bone surface versus 87% in the tibia). These findings highlight a specific mandibular response to OVX, in particular fewer microarchitectural alterations compared to that in the tibia. For the latter, the trabecular bone thickness and surface were correlated with the BMAT content. Oral functions may have a protective effect on the mandibular BMAT conversion in an OVX context.

Keywords: Rats; Mandible; Ovariectomy; Aging; Bone microarchitecture; Bone Marrow Adipose Tissue; Micro-CT

INTRODUCTION

Osteoporosis is a common and widespread skeletal disease that is characterized by an imbalance of bone remodeling that leads to a systemic loss of bone mass and in changes to the bone microarchitecture that occur in a site-specific manner [1]. The loss of gonadal function and aging are the two most important factors contributing to the development of the structural decay of the trabecular and cortical bone [2]. These skeletal alterations, which are both quantitative and qualitative, are most often described at the skeletal sites of fractures, such as the long bones of the appendicular skeleton (the epiphyses of the femur and the tibia in particular) and at the bones of the axial skeleton (vertebrae) [3]. Although several clinical studies have reported correlations between the changes in the bone mineral density (BMD) at the hip or spine, and in the changes in the alveolar and basal BMD in the mandible, other studies have shown conflicting results in an osteoporosis context [4,5]. In an ovariectomized rat model (mostly in young animals), a lower response to estrogen deficiency has been reported in the mandibular alveolar bone compared to that in the proximal metaphysis of the tibia, especially in the trabecular bone compartment [6,7]. Hence, the existence of osteoporosis of the cranio-facial skeleton and its impact on the teeth-bearing areas (alveolar bone) are still debated today [8,9]. In particular, there is still a lack of information on the bony changes in aged animals (mature skeleton) [10] and their relationships with local factors, such as bone marrow adipose tissue (BMAT) content and spatial distribution, whose potential regulatory roles in bone metabolism have been paid progressively more attention in the field [11].

We previously showed that the mandibular trabecular bone had a high density compared to that of the tibia which, in contrast, has a large surface area that is in contact with the bone marrow [12]. In addition to their close anatomical vicinity, the cells of the bone and the BMAT are critical for each other's functions that ensure bone homeostasis [13]. Bone marrow adipocytes (BMAds) are the most abundant differentiated stromal cells in human adult bone marrow, representing up to 70% of the marrow volume or 5-10% of the total weight of the whole body fat mass [14]. The hematopoietic cellularity of bone marrow decreases with age with a corresponding increase in the fat fraction [15]. Bone marrow adipose conversion, resulting from the differentiation of skeletal stem cells (SSCs), appears to be a tightly

regulated process [16]. The BMAT content has been reported to vary in several physiopathological contexts, such as aging [17] or postmenopausal osteoporosis [18,19], and it has also been reported to be inversely correlated to the trabecular bone volume and resorption surface in iliac crest bone biopsies, thus playing a key role in the regulation of bone turnover [20,21]. Several magnetic resonance imaging (MRI) studies have reported, in osteoporotic women, a higher bone marrow fat fraction (BMFF), mainly in the vertebrae and the long bones [17,22]. This increase was found to be inversely related to bone formation (osteoblastic activity) during osteoporosis, supporting the hypothesis that a preferential differentiation of SSCs toward the adipogenic pathway occurs at the expense of the osteogenic pathway [18]. In addition, a decrease in the unsaturation index of the BMFF has also been reported [19], as well as an increase in the content of pro-inflammatory cytokines (i.e., IL-6 and TNFα) and adipogenic markers (i.e., adiponectin and soluble RANKL) within the bone marrow supernatant fluid of osteoporotic patients, leading to increased bone fragility [23]. The bone marrow adiposity (BMA) is thus recognized as a major metabolic actor in the pathophysiology of osteoporosis [24,25].

The distribution of BMAT in the skeleton reveals site specificities [26–30]. In rodents, the content and composition of BMAT have been reported to be distributed differently between the distal and proximal metaphysis of the tibia [31] and also between the lumbar and caudal vertebrae [32]. In addition, a preferential location of BMAds has been reported among human iliac crest bone biopsies in different physiopathological contexts: stacked in the paratrabecular areas in osteoporosis and in the central bone marrow areas in plasmocytoma [33]. Moreover, bone marrow stromal cell (BMSC) progenitors residing close to the bone surface in long bones (tibiae) have been reported to be functionally distinct from those in the central bone marrow, suggesting a differential metabolic activity according to the distribution pattern of the BMAds [34]. In preclinical osteoporosis models, ovariectomy-induced trabecular bone loss was observed with distinct patterns according to the location within the tibia [29]. In addition, BMAT increased with osteoporosis, while the trabecular bone volume decreased, suggesting an inverse relationship between osteogenesis and adipogenesis [16,18] and arguing for an involvement of BMAT in the impairment in the osteoresorption-osteoformation balance [35,36].

Mandibular bone loss remains understudied and could be triggered, during aging and osteoporosis, by variations in the BMAT content and composition [37]. BMAT could represent an early biomarker of the occurrence and progression of the osteoporotic status, and it has been insufficiently explored clinically [22,37,38]. In the present study, we used an original methodology for the simultaneous 3D assessment of the bone microarchitecture [39] BMAT content and spatial distribution [12]. The objectives of the present study were as follows: i) to assess the long-term changes in the mandibular bone microarchitecture, BMAT content and spatial distribution during aging and after ovariectomy in a mature rat model and to compare these parameters with the proximal metaphysis of the tibia, and ii) to analyze whether these parameters are correlated within the functional alveolar and condylar areas of the mandible. In addition, differences in the masticatory activity between the experimental and control groups were taken into account by standardizing the food intake. This standardization was achieved by correcting of the transient hyperphagia in the ovariectomized animals by setting a long-term pair-feeding protocol consisting of providing equal food intake with that of the SHAM groups. Thus, the specificities between the alveolar bone and condylar regions within the mandible were explored in conditions where the diet was controlled (OVX _PF groups) or not (OVX_AL groups).

MATERIAL AND METHODS

Animal Procedures

Six-month-old female Sprague-Dawley rats (*rattus norvegicus,* n=69) were used in this study (Janvier Lab, Laval, France). The provider reported that the rats were free of known viral, bacterial and parasitic pathogens. Animals were randomly assigned prior to the operation by the provider in three distinct groups: the OVX_AL (n=20), OVX_PF (n=20) and SHAM groups (n=29). OVX_AL and SHAM groups were fed *ad libitum* (free access to tap water and a standard diet). A pair-feeding protocol was maintained until the sacrifice of the animals. All experiments on animals were carried out with the approval of the French Ministry of Research and Innovation (approval no. APAFIS#4197-2015091514435707). Animal procedures were performed in an accredited animal facility (authorization no. B5935010) at the University of Lille with the approval of the Animal Ethics Committee and in accordance with the directive 2010/63/EU and the "Principles of Laboratory Animal Care" recommended by the National Society for Biomedical Research in France. Rats (n=3/cage according to the EU laws) were housed in type 4 cages filled with Lignocel® (hygiene animal bedding) enriched with horizontal tubes for climbing and were kept under controlled conditions at 22±2°C on a 12 h light/12 h dark cycle with lights on from 07.00 a.m to 7.00 p.m. Rats were euthanized by exsanguination under anesthesia at 6 months (baseline, n=9), 10 months (M4 post-OVX, n=9) and 15 months of age (M9 post-OVX, n=11). At sacrifice, the right hemimandibles and tibias were harvested, immediately fixed for 48 h in 10% neutral-buffered formalin and stored in phosphate buffered saline prior to further micro-CT analyses.

Micro-CT image acquisition and reconstruction: SCAN1

To simultaneously assess the bone microarchitecture and the BMAT content, the trabecular area was investigated in three skeletal locations: (i) the intraradicular alveolar bone of the first molar; (ii) the central area of the mandibular condyle in the mandibles and (iii) the secondary spongiosa of the tibial metaphysis. All bone samples were scanned for the first time (i.e., SCAN1) to allow the analysis of the trabecular bone morphometric parameters. Specimens (mandibles and tibiae) were placed in a plastic sample holder and were scanned using a Skyscan 1172 micro-CT device (BRUKER, Kontich, Belgium) with the software suite

provided by the manufacturer. Scan settings were as follows: isotropic voxel size 10µm^3, 80 kVp, 100 µA, Al-Cu filter, 2400 ms integration time, and 0.5° rotation step over 180°. For the reconstruction, the following settings were applied: Gaussian smoothing, ring artifact reduction 6, and beam hardening correction 50%. After the first acquisition, the samples were prepared for BMAT analysis [12] and were scanned a second time (SCAN2) to allow the analysis of the BMAT parameters using the same acquisition settings as the first scan. Briefly, each sample was decalcified and stained in a 1% osmium tetroxide solution (stabilized with a 2.5% potassium dichromate solution).

Osmium tetroxide staining protocol

After SCAN1, the samples were prepared for BMAT analysis. Thus, all the bone samples were decalcified under controlled slow oscillations in 4% formic acid/10% NBF (1:1), pH 7.4, for 4 days. Once the bones were demineralized, they were rinsed in distilled water. Each decalcified bone was then stained in the fume hood for 48 h in an aqueous staining solution that was composed of a 1% osmium tetroxide solution that was stabilized in a 2.5% dichromate potassium solution at room temperature. Then, the stained bones were rinsed twice in PBS for 3 h each at room temperature and a last wash was performed in the hood overnight. Osmium stained bones were then moved to a fresh set of 50 ml falcon tubes containing 45 ml of PBS each and were stored at 4°C until the micro-CT acquisition.

Micro-CT image acquisition and reconstruction: SCAN 2

After osmium tetroxide staining, the decalcified and stained bone samples were scanned a second time (i.e., SCAN2) to allow the analysis of the BMAT. Samples were scanned using the same acquisition settings as the first scan. For the reconstruction of the SCAN2 datasets, the following settings were applied to reveal the osmium-stained BMAT: Gaussian smoothing, ring artifact reduction 3, and beam hardening correction 30%.

Image datasets alignment (SCAN1 and SCAN2 registration)

The SCAN1 and SCAN2 datasets were rotated to obtain the same orientation, which was specific for each skeletal location (the longitudinal axis of the proximal metaphysis in the tibia and the mandibular condyle and the first molar in the alveolar ridge for the mandible).

Then, the reoriented datasets of each sample (SCAN1 as the reference, SCAN2 as the target) were manually registered using the Dataviewer software (v. 1.5.2.4) following these critical steps: (i) the coregistration of the global outlines; (ii) the adjustment of the enamel of the rodent incisor (in the case of the alveolar ridge) and (iii) the progressive adjustment of the trabecular network and bone marrow space using the profile scale diagram and different angles of view.

Determination of the Regions of Interest (ROI)

After registration, the regions of interest (ROI) were drawn in the SCAN1 datasets that delineated the trabecular area of the samples using CTAn. For the alveolar ridge, the ROIs were selected as the intraradicular bone of the first molar from the furcation to the apex roots, as adapted from the protocol of Du et al. (modification: an oval shape was used instead of a circular one) [40]. In the condyle, the ROI was selected according to the method described by Jiao et al., as a rectangle shape (1 mm length, and 0,5 mm height) in the central compartment [41]. In the proximal tibia, 200 cross-sections (2 mm height) were selected 1.5 mm under the growth plate, and the trabecular area was isolated from the cortical area by a semiautomated protocol in CTAn© [42].

Micro-CT image analysis - trabecular bone microarchitecture

In the ROIs of the SCAN1 datasets, a one-level Otsu's method was used to determine the threshold between the mineralized tissue and the bone marrow compartment (and vice versa) [43], and the following bone microarchitectural parameters, reflecting the morphology of the trabecular network for each skeletal location, were measured using CTAn©: percent bone volume (BV/TV, %), trabecular bone surface/volume ratio (BS/TV, mm^{-1}), trabecular number (Tb.N, mm^{-1}), trabecular thickness (Tb.Th, mm), trabecular separation (Tb.Sp, mm) and trabecular pattern factor (Tb.Pf, mm^{-1}).

Micro-CT image analysis – BMAT content and distribution

For the quantification of the BMAT content, each defined ROI of the SCAN1 datasets was reused on the coregistered SCAN2 dataset to determine the BMAT content in the same area that the bone microarchitecture was assessed. For the mandibular bone, a fixed-threshold value (between 110 and 255 grayscale levels) was used for both skeletal locations. In the tibia, the BMAT was segmented using a multilevel Otsu algorithm (3 levels). The following BMAT parameters were measured for each skeletal location: the percentage of adipocyte volume in the total volume of the ROI (Ad.V/TV, %) and, in using an original method, the ratio adipocyte volume/marrow volume (Ad.V/Ma.V, %). To assess the spatial distribution profile of BMAT in relation to the bone surface, a customized stepwise process was created in CTAn© to plot the percentage of BMAT *vs* the distance from the trabecular bone surface. After uploading the segmented osmium-stained BMAT from the SCAN2 datasetsas 'the image" and the binarized-trabecular network of the SCAN1 datasets as "ROI", this task list combines the repetition of the following tasks 5 times: a one-level Otsu thresholding, a morphological operation (20 µm 3D dilatation step = 2 pixels), a saving image and a 3D morphological analysis to determine the percentage of BMAT in each volume.

Statistical analyses

All statistical analyses were performed with the SAS package software©, release 9.4 (SAS Institute, Cary, NC). Continuous variables are described by the mean and standard deviation, or the median and interquartile range. The normality of the distributions was evaluated graphically and using the Shapiro-Wilk test. Animal body weight was compared between the groups, week by week, using a linear mixed model to account for the correlation between the repeated measures within subjects by including a random subject effect.

The parameters of the trabecular bone microarchitecture and BMAT content were compared among the three time points (baseline, M4, M9) in the SHAM group for each skeletal location (the proximal metaphysis of the tibia, alveolar bone and condyle) with a linear mixed model with a random subject effect.

The parameters of the bone microarchitecture and BMAT were compared among the three groups (SHAM, OVX_AL, OVX_PF) within each skeletal location and at M4 and M9 with a linear mixed model with a random subject effect. In the case of significant results, post hoc comparisons between the groups were performed.

Associations between the trabecular bone microarchitectural parameters and BMAT parameters were assessed for each skeletal location using the Spearman correlation coefficient in the SHAM group and in the pooled OVX groups.

The spatial distribution of the BMAT content was compared among the groups by localization and time (M4 and M9) using an analysis of covariance model adjusted for the animal's weight. In the case of significant results, post hoc comparisons between the groups were performed. The statistical significance for all tests was set at $p < 0.05$.

Principal Component Analysis

The micro-CT data were processed with Principal Component Analysis (PCA) [44]. PCA is described as a "unsupervised" method that explores the variability within a dataset. This statistical multivariate analysis tool allows for the study of the relationships among the variables (BV/TV, Ad.V/Ma.V etc.) and the samples of the groups (SHAM and OVX) at the different postsurgery observational times (baseline, M4, and M9). PCA was performed with the PLS Toolbox v. 6.7 (Eigenvector Research Inc., West Eaglerock Drive, Wenatchee, WA, 98801) operating in the MATLAB R2010a environment (Mathworks Inc., Natick, MA, USA). Prior to PCA, the autoscale function was applied to the dataset.

RESULTS

Animal body weight

The average weight of the animals before surgery was 346.3 ± 9 g (Fig. 1). From the second week after OVX, a weight difference of approximately 10% was observed between the animals of the OVX_AL group and those of the SHAM group (403.6 ± 19 g *vs* 363.9 ± 12 g, $p < 0.001$), highlighting a rapid weight gain after OVX. This was followed by a slower weight gain from week 8 to week 40 (after transient hyperphagia, which was observed until 8 weeks post-surgery). This weight difference was not found between the OVX_PF and the SHAM group at 2 weeks post-OVX (382.4 ± 10 g *vs* 363.9 ± 12 g, $p=0.10$).

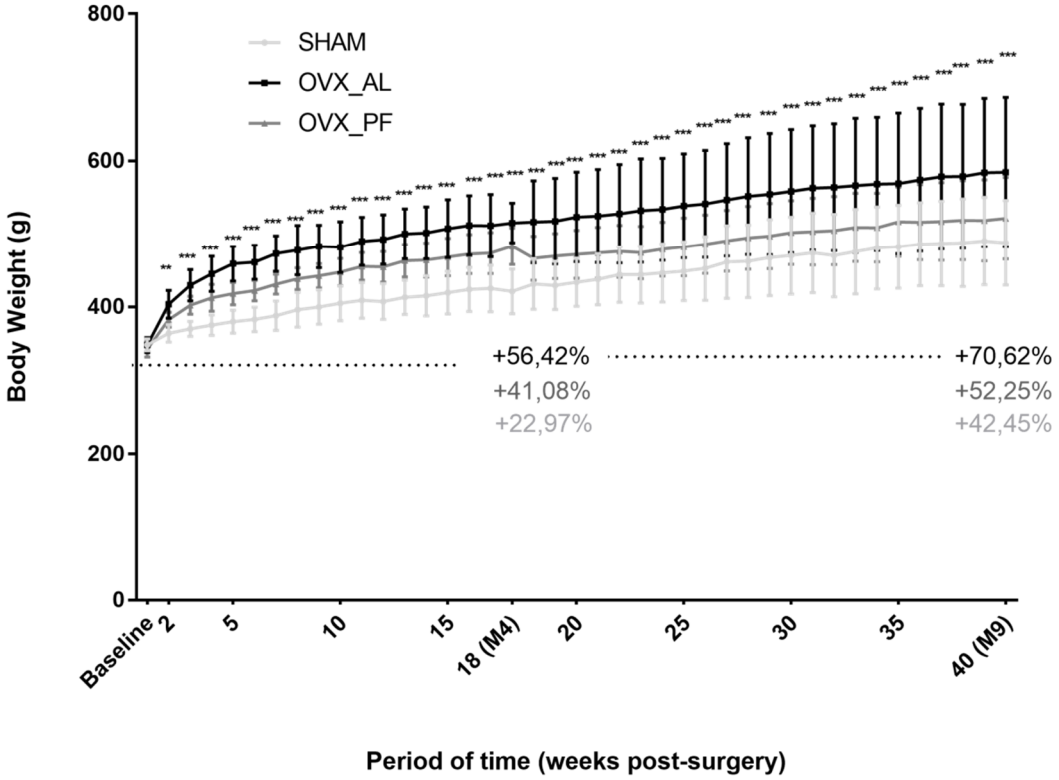

225

226 **Figure 1 : Animal body weight differences from week 0 to week 40 in SHAM, OVX_AL and**
227 **OVX_PF rats. Values are means ± SD. Differences between groups are shown: ** p<0.01,**
228 ***p<0.0001.**

229

Trabecular bone microarchitecture

In the SHAM group, no significant differences related to aging were observed in the trabecular bone microarchitectural parameters regardless of the skeletal location (alveolar bone, condyle, and tibia – Fig. 2).

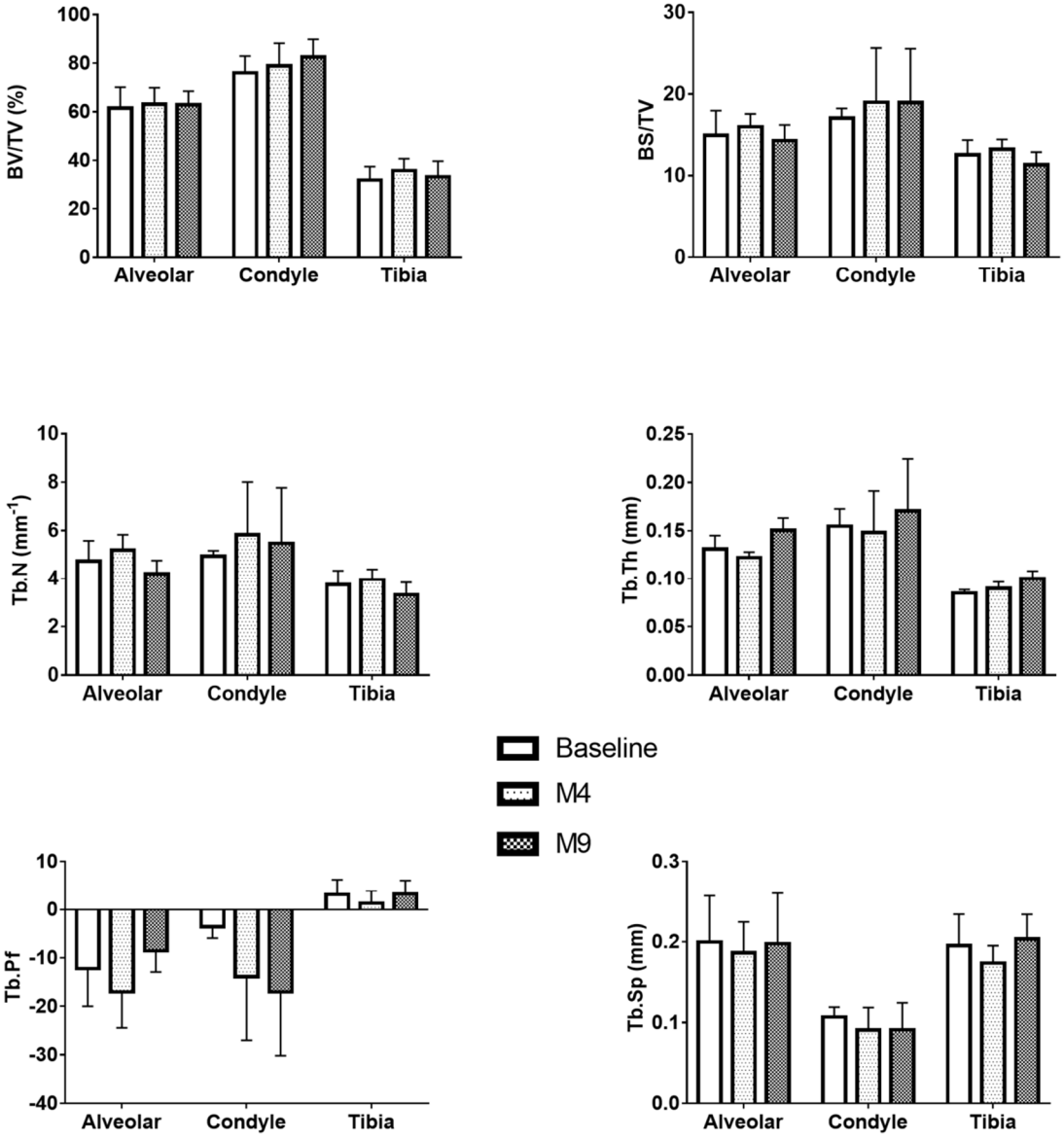

Figure 2 : No age-related effects on trabecular bone microarchitecture whatever skeletal sites (alveolar bone, condyle, tibia) in the SHAM groups respectively at baseline, M4 and M9. Values are means ± SD.

The trabecular bone microarchitectural parameters were significantly modified between the SHAM and OVX groups according to the skeletal locations. However, no differences were observed in the trabecular bone microarchitectural parameters between the OVX_AL and OVX_PF groups at M4 and M9, regardless of the skeletal location (Figs. 3-Additional Fig. 8). In the tibia, at M4, significant modifications in both of the OVX groups were observed compared to those of their SHAM counterparts: the trabecular BV/TV was 62% lower, Tb.N was 64% lower and both Tb.Th. (+10%, $p<0.0001$) and Tb.Sp. were higher (+65%, $p<0.001$) in the OVX groups compared to those of the SHAM group. In addition, the Tb.Pf. was approximately 10-fold higher ($p <0.0001$) in the OVX group compared to that of the SHAM group. No changes in the microarchitectural parameters were observed between M4 and M9 (see Additional Fig. 8).

In the alveolar bone (Fig. 3), significant modifications in both of the OVX groups were observed compared to those of their SHAM counterparts: BV/TV was 15% lower at M4 and 20% lower at M9 ($p <0.0001$), Tb.N. was 19% lower at M4 post-OVX ($p <0.0001$) in the OVX groups compared to that of the SHAM group. The Tb.Th. did not change regardless of the time post-OVX. The OVX groups were also characterized by a higher Tb.Sp. (+10% at M4, $p<0.0001$ and +28.5% at M9, $p<0.0001$) compared to that of the SHAM group.

In the condyle (Fig. 3), no significant changes in the trabecular BV/TV were observed at M4 or M9 post-OVX. However, the OVX groups were characterized by a lower Tb.N. (up to -35% at M9, $p<0.001$) compared to that of the SHAM group. In addition, when comparing the OVX groups to the SHAM group, we observed a higher Tb.Th. (+26% at M9, $p= 0.027$), which was associated with a more than 6-fold increase in the Tb.Pf. ($p = 0.002$) and a higher Tb.Sp. at M9 (+40%, $p = 0.040$).

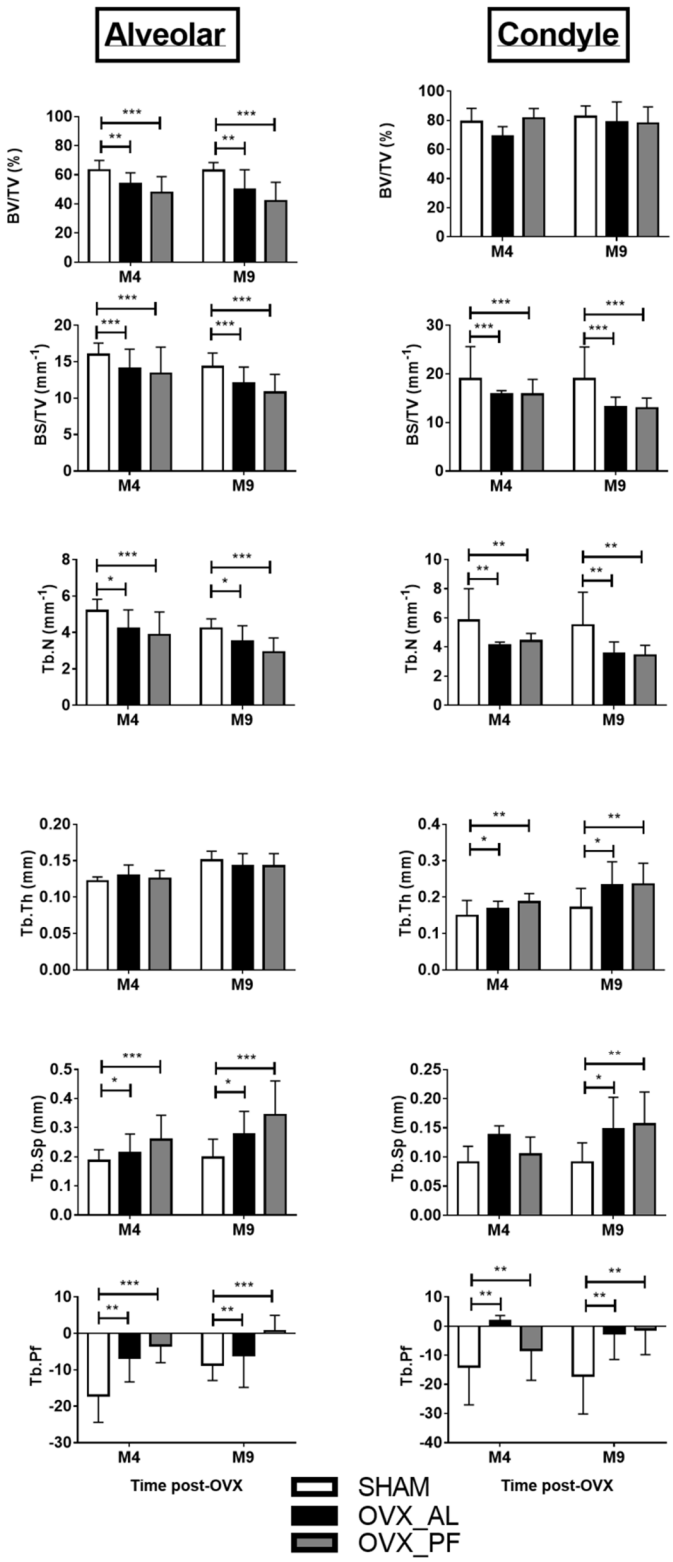

264

265 **Figure 3 : OVX-related effects on trabecular bone microarchitecture in the alveolar bone**
266 **(left) and in the condyle (right) respectively at M4 and M9. Values are means ± SD.**
267 **Differences between groups are shown: *p<0.05, **p<0.01, *** p<0.0001**

268

BMAT content

In the SHAM group (Fig. 4), no age-related changes in the BMAT content (Ad.V/Ma.V, %) were observed in both mandibular sites, but there was a 2-fold significant increase in the BMAT content in the tibia at M4 post-OVX compared to that at baseline and a significant decrease of -30% at M9 compared to that at M4 post-OVX.

In the mandible, no BMAT content was found in the condyle regardless of the age of the animals in the SHAM group. Interestingly, at baseline, the BMAT content in the tibia exhibited a significantly 10-fold increase compared to that of the alveolar bone.

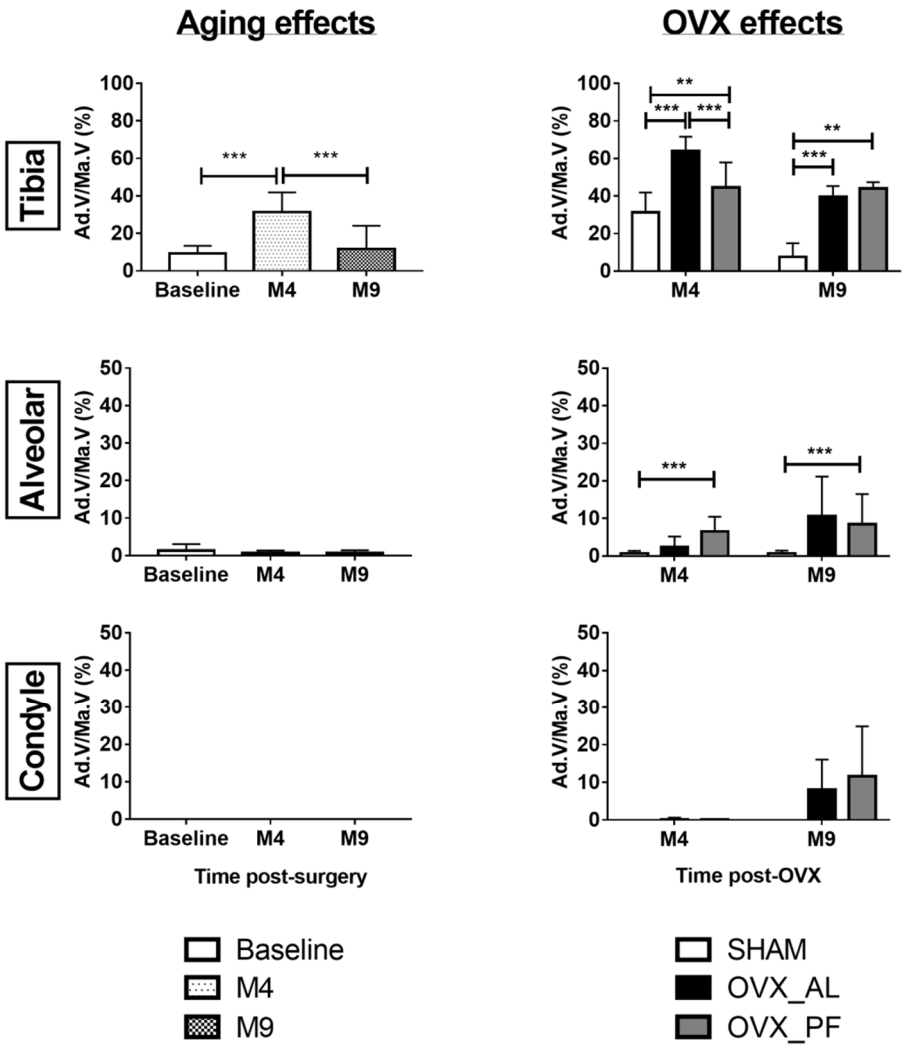

Figure 4 : Age and OVX-related effects on BMAT content (Ad.V/Ma.V: adipose volume/marrow volume, %) respectively at baseline, M4 and M9 in the 3 skeletal locations (tibia, alveolar bone, condyle). Values are means ± SD. Differences between groups are shown: * p <0.05, ** p <0.01, *** p <0.0001

After OVX (Fig. 4), the bone loss observed in the tibia was accompanied by an increase in the BMAT content at M4 and M9 compared to that of the SHAM group. Indeed, there was a significant increase in the Ad.V/Ma.V compared to that of the age-matched SHAM group (+51% at M4, $p<0.0001$ and +337% at M9, $p<0.0001$). In the alveolar bone, bone loss was accompanied by a significant increase in the Ad.V/Ma.V compared to that of the age-matched SHAM group, but this effect was only observed in the OVX_PF group (+1908% at M4, $p<0.0001$, and +1256% at M9, $p<0.0001$). In the condyle, no bone loss was found, but small amounts of adipose content appeared at M4 post-OVX (approximately 1% of the available marrow volume) and reached 10% at M9 post-OVX. The micro-CT 3D renderings of the alignment of the bone microarchitecture and BMAT content are illustrated at each skeletal site during aging and OVX in additional figures 9-10-11.

BMAT spatial distribution

Figure 5 illustrates the spatial distribution of BMAT within the proximal tibia, alveolar bone and condyle, which was calculated as the distance from the trabecular bone surface, up to 100 µm away [12]. In the tibia, BMAT was preferentially in contact with the trabecular bone surface after ovariectomy. Indeed, 87% of the trabecular bone surface was covered by BMAds at M4 in OVX_AL group versus 40% in the SHAM group ($p=0.008$). A higher BMAT content was found in contact with the trabecular bone surface at M9 in both OVX_PF group (48%) and OVX_AL group (52%) compared to the SHAM group (13%, $p<0.0001$). In contrast, in both mandibular sites, the small amount of BMAT remained distributed within the entire marrow spaces with less than 5% of the trabecular bone surface covered by BMAds whatever the time post-OVX.

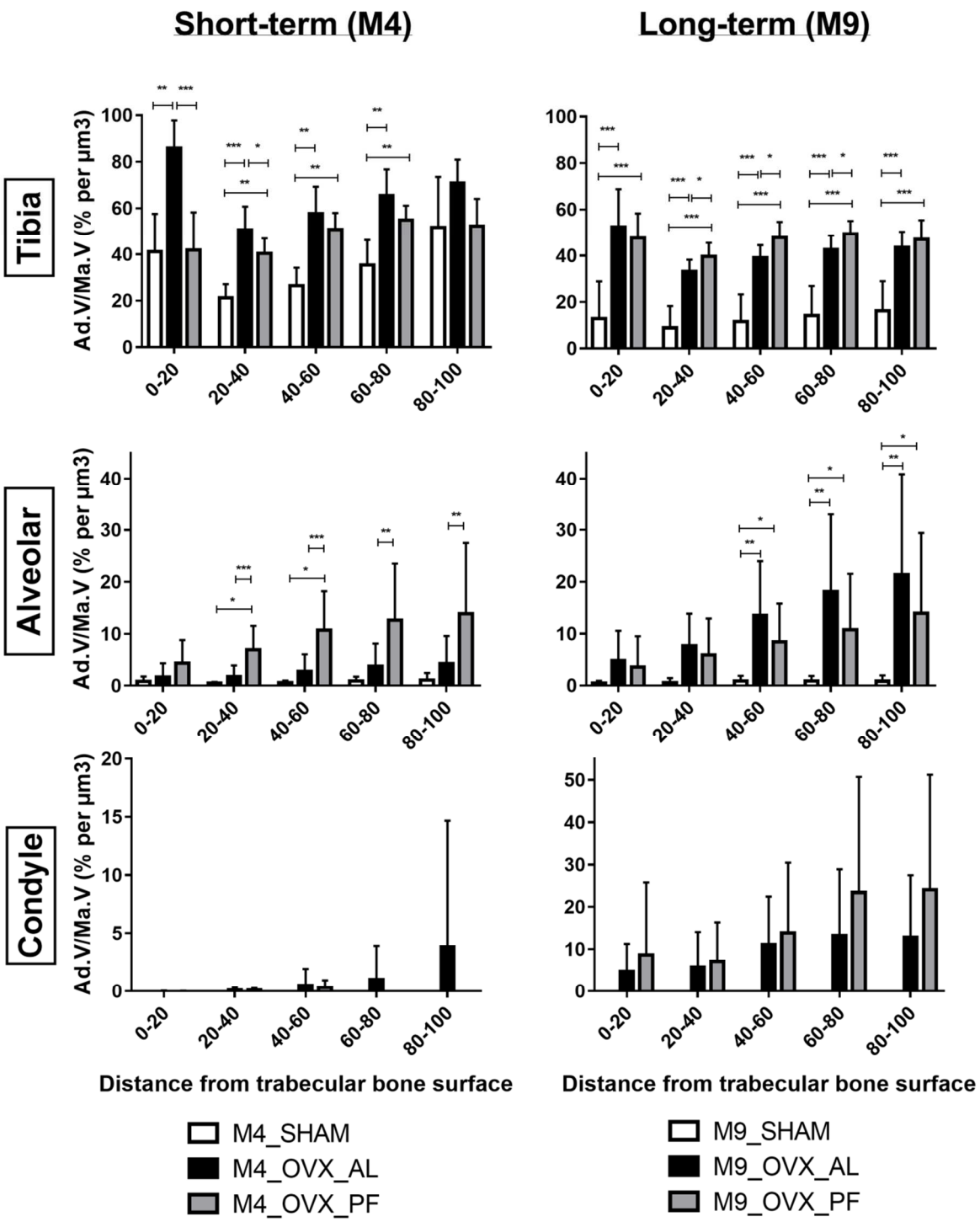

305

306 **Figure 5 : BMAT spatial distribution at M4 (left) and M9 (right) for each skeletal locations.**
307 **Values are means ± SD. Differences between groups are shown: *p<0.05, **p<0.001,**
308 ***p<0.0001**

Relationship between bone microarchitecture and BMAT variables

The global relationship among the micro-CT variables and groups (SHAM and OVX) was explored with principal component analysis (PCA). In the tibia, the score plot (Fig. 6A) shows two clusters that were formed by the SHAM group (right) and the OVX groups (left). This separation was made along PC1 (72.26%). No PCA-based separations between the OVX groups were observed. The loading plots (Fig. 6B) show that the BV/TV, BS/TV and Tb.N were higher in the SHAM group than in the OVX groups. The values of the Tb.Pf, Tb.Sp, Tb.Th, and Ad.V/Ma.V were higher in the OVX groups than in the SHAM group.

The PCA was also conducted on the datasets related to the mandibular variables. However, no clear and distinct separation was observed at either mandibular site.

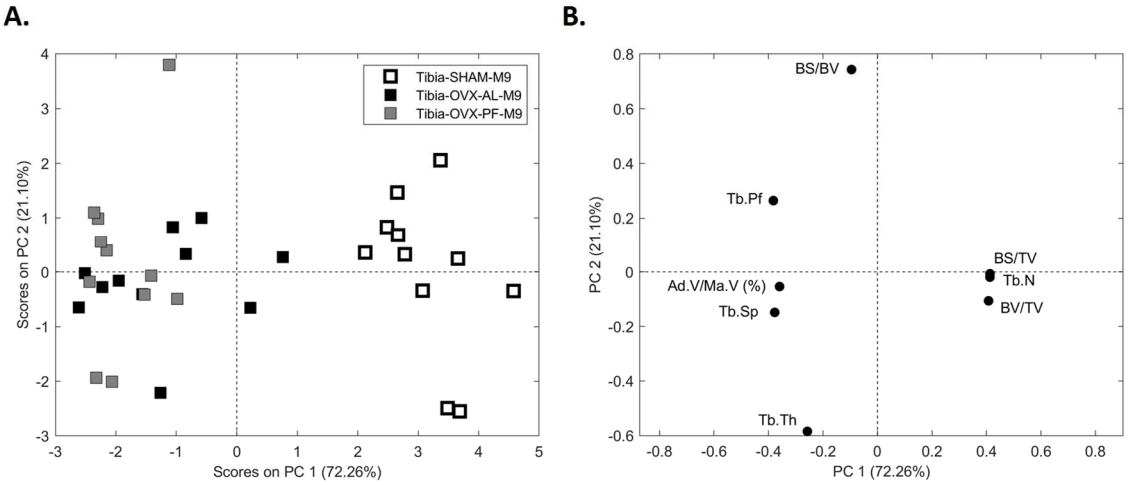

Figure 6 : Principal Component Analysis (PCA) in the tibia (M9).
A. Score plots, representing the distribution of samples in the space defined by PC1 and PC2, shows 2 distinct clusters associated to SHAM group (right) and OVX groups (left)
B. Loading plots, representing the contribution of each variable in the space defined by PC1 and PC2, shows the association of micro-CT variables that most characterized the SHAM groups (right) and both OVX groups (left).

Linear regression analysis (bivariate approach) was then carried out to explore the correlations between the microarchitectural and BMAT variables in the OVX and SHAM groups, at the various time-points postsurgery. No correlations among the bone microarchitectural and BMAT parameters were found in the SHAM group (data not shown). However, in the OVX groups, for the tibia only, significant correlations were found between the Ad.V/Ma.V and Tb.Th (r=-0.55, p=0.0003) and between the Ad.V/Ma.V and BS/BV (r=0.52, p=0.0006) (Fig. 7).

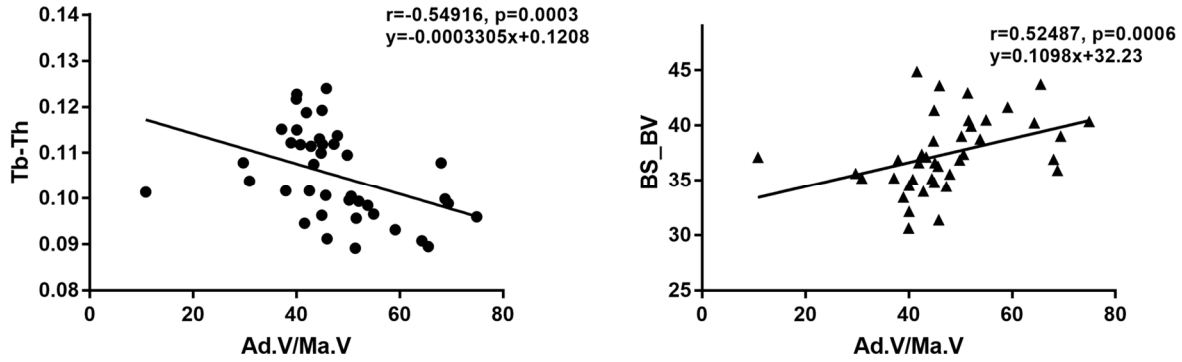

Figure 7 : Negative correlation between Tb.Th and Ad.V/Ma.V and positive correlation between BS/BV and Ad.V/Ma.V in the tibia among both OVX groups (OVX_AL and OVX_PF). The correlation coefficient, level of significance p and equation of the line are indicated (nonparametric Spearman rank correlation test).

DISCUSSION

The ovariectomized (OVX) rat model is now largely recognized as a suitable osteoporosis preclinical model for the assessment of mandibular bone microarchitecture [45]. In the rat mandible, the effects of OVX (estrogen depletion) on the alterations of the microarchitectural parameters in the alveolar bone and the condyle have been studied with various experimental conditions that make the interpretation of the existing data complex and incomplete, including the use of different rat strains, different areas of analysis in the mandible, different OVX delays and time post-OVX analyses. These studies also report contradictory data, making the analysis of the effects of aging, on the one hand, and OVX, on the other hand, unclear in the mandible [46–49]. With the use of our 3D micro-CT approach allowing alignment of the bone and the BMAT, the present study reports a comprehensive investigation in adult rats that simultaneously studied changes in the bone microarchitectural and BMAT content and its spatial distribution in the alveolar bone and the condyle in a controlled-diet condition, with a clear distinction of age and OVX status. Here, we show that once the rat skeleton is mature [10] (at 15 months of age), (i) aging does not impact the trabecular bone microarchitecture in both mandibular sites (the alveolar bone and condyle) nor in the tibiae in rats and (ii) OVX has a distinct skeletal impact not only on the mandibular bone microarchitecture but also on the mandibular BMAT content (4-6-fold lower compared to that of the metaphyseal tibial area) and spatial distribution (BMAT remained at a further distance from the trabecular bone surface compared to that of tibia).

The absence of microarchitectural differences may be due to the advanced age reached by the animals at baseline (6 months) and by a slower remodeling rate that has been reported with advanced age. These hypotheses are consistent with a study of Kribbs *et al.* showing that the decrease in the mandibular bone mass was not correlated with age [50]. Although some authors reported a lower proliferative capacity and a lower osteogenic differentiation of skeletal stem cells (SSCs) with age [51–53], other data indicate that there are no changes in the differentiation capacities of SSCs with age in rats [54], suggesting that the effect of aging may not be synchronized through the whole skeleton. Previous data show that the remodeling activity becomes predominant in rat trabecular bone areas after 6 months of age, suggesting that the skeletal dynamics of rodents may be more relevant to those in the

adult human situation than it was previously thought [55,56]. Indeed, it has been shown that, similar to higher mammals, the prevailing activity in the tibial trabecular bone of aged (12-month-old) rats is remodeling and not modeling [57].

We also show that, in rats of 10 months of age, OVX-induced mandibular bone loss was three-fold lower than the proximal metaphyseal bone loss in the tibia and was observed only in the alveolar bone (not in the condyle). In Wronski's work, osteopenia was detected in OVX rats as early as 14-days post-OVX in the tibia and became progressively more pronounced up to 100 days [2]. Afterwards, the tibial trabecular bone volume appeared to stabilize (decreased bone loss and bone formation/resorption indices that were only marginally enhanced). In the present study, no OVX-induced microarchitectural changes were observed between M4 and M9; hence, we mainly observed an "early" and "fast" reaction of the body to the surgery (estrogen deficiency) in rats [58,59]. In addition, consistent with previous findings, our data show that mandibular bone loss is significantly less important than that in the proximal tibia in response to OVX [6,8,60], suggesting that oral functions may induce stress on mandibular bone cells and prevent oral bone loss. Interestingly, OVX also induced a smaller Tb.N and Tb.Th decrease in both mandibular sites compared to that in the tibia. This small mandibular response to OVX in rodents can be partially explained by the dense trabecular bone network (at baseline) in the mandible [12]. The small response may also be attributed to the unique skeletal characteristics of the mandible, both morphologically and functionally (with the presence of masticatory activity and a 10-fold higher remodeling activity in the alveolar and condylar regions compared to that in the tibia [61,62]) and embryologically (with the profile of mandibular skeletal stem cells described as being preferentially osteogenic [52,63]). In the present study, transitory hyperphagia was reported after OVX, but it did not induce any changes in the bone microarchitectural parameters in rats, which is in accordance with Jiang's findings, who also reported that there was no impact on the bone strength [64]. Bearing in mind that the mandible does not represent a typical fracture site in the skeleton, these observations could explain its resistant behavior even in an estrogen-depletion context.

In addition to the specific mandibular response to OVX, we reported distinct changes in the BMAT content and spatial distribution in the alveolar bone and condyle sites during OVX compared to that in the proximal tibial metaphysis. Indeed, the mandible exhibited a

delayed increase in the BMAT content compared to that in the tibia, with a 4-6-fold lower BMAT content, suggesting a slower BMAT conversion rate in the mandible than in the tibia. Interestingly, an alveolar BMAT increase was observed only in the pair-feeding OVX groups, highlighting, for the first time, a protective effect of oral functions on the alveolar BMAT conversion. No age-related BMAT differences were observed at either mandibular site. In the tibia, age-related changes were observed and we believe that the 30% decrease in BMAT content at M9 compared to that at baseline may be due to the diaphyseal growth in the proximal direction that crosses the volume of interest (mainly hematopoietic bone marrow in the central trabecular areas) in aged animals. With the use of our 3D micro-CT approach that allowed us to align the bone and the BMAT [12], the present study highlights the features of the alveolar and condylar BMAT content and their spatial distribution after OVX in a rat model. Indeed, the spatial distribution of the mandibular BMAT was homogeneously distributed in the first 100 µm from the trabecular bone surface, whereas it was clearly preferentially distributed close to the trabecular bone surface in the tibia (87% of the trabecular bone surface covered by bone marrow adipocytes in the tibia *vs* approximately 5% in both mandibular sites). Bearing in mind the potential role of BMAT in bone metabolism, the distinct metabolic function of the mesenchymal progenitors that are located close to the bone surface and the bone formation areas (the superior proliferative ability and reduced expression of cell cycle inhibitors) reported by Siclari *et al.* may explain the differences in the BMAT content measured in the different skeletal locations in the present study and could provide support for a more metabolically active role of the BMAds in the tibia [34]. Our data highlight the importance of investigating not only the BMAT content but also the BMAT spatial distribution in relation to the bone surface and support the hypothesis of a potential role of the BMAds in bone metabolism.

The micro-CT variables provide biological information that demonstrates the effect of OVX, as shown by PCA (Fig. 6 A-B). These results show that the SHAM and OVX groups do not share the same microarchitectural characteristics. The OVX groups were characterized by a high BMAT content (Ad.V/Ma.V), larger trabecular thickness and trabecular separation as well as a more disconnected trabecular network compared to those of the SHAM group. The SHAM group was characterized by a high trabecular bone volume and number compared to

433 those of the OVX group. Interestingly, bivariate statistical analyses (linear regression)
434 showed only correlations in the OVX groups in the tibia between the bone
435 microarchitectural and BMAT parameters. The negative correlation that was found between
436 the Ad.V/Ma.V and Tb.Th may suggest the involvement of the BMAT content in the
437 trabecular bone thinning in an OVX context. In addition, the positive correlation between the
438 Ad.V/Ma.V and BS/BV has been reported as an excellent predictor of bone loss. No
439 correlations were found in the OVX groups at the mandibular sites, suggesting that BMAT
440 has a smaller impact on trabecular bone loss than that at other sites. The differences in the
441 BMAT content, which were only observed after OVX in the pair-fed group, demonstrate a
442 probable protective role of oral functions in alveolar BMAT conversion.

443 The investigation and understanding of the relationship between BMAT and the bone quality
444 has emerged as an exciting challenge in research in recent years (70-85% of the trabecular
445 bone surface is in contact with the bone marrow). It now appears evident that BMAT should
446 be kept in mind and considered when assessing the bone quality parameters [65]. By
447 measuring the bone and BMAT within the same region of interest, our data highlight the
448 specific response of the mandibular microarchitecture, BMAT content and spatial
449 distribution during OVX. The distribution pattern of BMAT in the three skeletal locations
450 demonstrates the importance of local factors in the regulation of bone metabolism, in
451 particular BMAT. It would be of great interest to precise the impact of these BMAT changes
452 on the bone quality at the tissue level.

453 In summary, OVX was characterized by marked microarchitectural and BMAT changes in the
454 tibia with significant correlation between the BMAT content and trabecular bone thickness
455 as well as clustering of BMAT close to the trabecular bone surface. By contrast, OVX was
456 characterized by few microarchitectural and BMAT content changes in both mandibular
457 sites, without any correlations between microarchitectural and BMAT variables. According to
458 these data, oral functions may have a protective effect on the BMAT conversion in the
459 alveolar bone in a context of estrogen depletion. These highlights underline the importance
460 of clarifying the long-term effects of local factors, such as the specific BMAT distribution on
461 the mandibular bone quality at the molecular level.

462

ACKNOWLEDGEMENTS

The authors thank the staff of the animal care facility (DHURE, Lille, France) for supplying the help on animal procedures. This study was supported by the French Society of Rheumatology (SFR). GK acknowledges the Research Foundation - Flanders for her postdoctoral grant (FWO/12R4315N) and her travel grant for a 6-months stay abroad in the PMOI lab.

CONFLICT OF INTERESTS STATEMENT: none

REFERENCES

1. Rachner, T. D., Khosla, S. & Hofbauer, L. C. Osteoporosis: now and the future. *The Lancet* **377**, 1276–1287 (2011).
2. Wronski, T. J., Cintrón, M. & Dann, L. M. Temporal relationship between bone loss and increased bone turnover in ovariectomized rats. *Calcif. Tissue Int.* **43**, 179–183 (1988).
3. Francisco, J. I., Yu, Y., Oliver, R. A. & Walsh, W. R. Relationship between age, skeletal site, and time post-ovariectomy on bone mineral and trabecular microarchitecture in rats. *J. Orthop. Res.* **29**, 189–196 (2011).
4. Jeffcoat, M. The Association Between Osteoporosis and Oral Bone Loss. *J. Periodontol.* **76**, 2125–2132 (2005).
5. Guiglia, R. *et al.* Osteoporosis, jawbones and periodontal disease. *Med. Oral Patol. Oral Cir. Bucal* **18**, e93-99 (2013).
6. Mavropoulos, A., Rizzoli, R. & Ammann, P. Different Responsiveness of Alveolar and Tibial Bone to Bone Loss Stimuli. *J. Bone Miner. Res.* **22**, 403–410 (2007).
7. Liu, X. L., Li, C. L., Lu, W. W., Cai, W. X. & Zheng, L. W. Skeletal site-specific response to ovariectomy in a rat model: change in bone density and microarchitecture. *Clin. Oral Implants Res.* n/a-n/a (2014). doi:10.1111/clr.12360
8. Mavropoulos, A., Kiliaridis, S., Rizzoli, R. & Ammann, P. Normal masticatory function partially protects the rat mandibular bone from estrogen-deficiency induced osteoporosis. *J. Biomech.* **47**, 2666–2671 (2014).
9. Devlin, H. Identification of the Risk for Osteoporosis in Dental Patients. *Dent. Clin. North Am.* **56**, 847–861 (2012).
10. Jee, W. S. & Yao, W. Overview: animal models of osteopenia and osteoporosis. *J. Musculoskelet. Neuronal Interact.* **1**, 193–207 (2001).
11. Hardouin, P., Rharass, T. & Lucas, S. Bone Marrow Adipose Tissue: To Be or Not To Be a Typical Adipose Tissue? *Front. Endocrinol.* **7**, (2016).

12. Coutel, X. *et al.* A Novel microCT Method for Bone and Marrow Adipose Tissue Alignment Identifies Key Differences Between Mandible and Tibia in Rats. *Calcif. Tissue Int.* (2018). doi:10.1007/s00223-018-0397-1

13. Hardouin, P., Pansini, V. & Cortet, B. Bone marrow fat. *Joint Bone Spine* **81**, 313–319 (2014).

14. Gimble, J. M., Robinson, C. E., Wu, X. & Kelly, K. A. The function of adipocytes in the bone marrow stroma: an update. *Bone* **19**, 421–428 (1996).

15. Guillerman, R. P. Marrow: red, yellow and bad. *Pediatr. Radiol.* **43**, 181–192 (2013).

16. Justesen, J., Stenderup, K., Eriksen, E. F. & Kassem, M. Maintenance of Osteoblastic and Adipocytic Differentiation Potential with Age and Osteoporosis in Human Marrow Stromal Cell Cultures. *Calcif. Tissue Int.* **71**, 36–44 (2002).

17. Justesen, J. *et al.* Adipocyte tissue volume in bone marrow is increased with aging and in patients with osteoporosis. *Biogerontology* **2**, 165–171 (2001).

18. Verma, S., Rajaratnam, J. H., Denton, J., Hoyland, J. A. & Byers, R. J. Adipocytic proportion of bone marrow is inversely related to bone formation in osteoporosis. *J. Clin. Pathol.* **55**, 693–698 (2002).

19. Yeung, D. K. W. *et al.* Osteoporosis is associated with increased marrow fat content and decreased marrow fat unsaturation: A proton MR spectroscopy study. *J. Magn. Reson. Imaging* **22**, 279–285 (2005).

20. Lips, P., van Ginkel, F. C. & Netelenbos, J. C. Bone marrow and bone remodeling. *Bone* **6**, 343–344 (1985).

21. Martin, R. B. & Zissimos, S. L. Relationships between marrow fat and bone turnover in ovariectomized and intact rats. *Bone* **12**, 123–131 (1991).

22. Paccou, J., Hardouin, P., Cotten, A., Penel, G. & Cortet, B. The Role of Bone Marrow Fat in Skeletal Health: Usefulness and Perspectives for Clinicians. *J. Clin. Endocrinol. Metab.* **100**, 3613–3621 (2015).

23. Pino, A. M. *et al.* Concentration of adipogenic and proinflammatory cytokines in the bone marrow supernatant fluid of osteoporotic women. *J. Bone Miner. Res.* **25**, 492–498 (2010).

24. Hardouin, P., Marie, P. J. & Rosen, C. J. New insights into bone marrow adipocytes: Report from the First European Meeting on Bone Marrow Adiposity (BMA 2015). *Bone* **93**, 212–215 (2016).

25. Eerden, B. van der & Wijnen, A. van. Meeting report of the 2016 bone marrow adiposity meeting. *Adipocyte* **0**, 1–10 (2017).

26. Kawai, M., de Paula, F. J. A. & Rosen, C. J. New insights into osteoporosis: the bone–fat connection. *J. Intern. Med.* **272**, 317–329 (2012).

27. Devlin, M. J. & Rosen, C. J. The bone–fat interface: basic and clinical implications of marrow adiposity. *Lancet Diabetes Endocrinol.* **3**, 141–147 (2015).

28. Lanske, B. & Rosen, C. Bone Marrow Adipose Tissue: The First 40 Years. *J. Bone Miner. Res.* **32**, 1153–1156 (2017).

29. Li, M., Shen, Y., Qi, H. & Wronski, T. J. Comparative study of skeletal response to estrogen depletion at red and yellow marrow sites in rats. *Anat. Rec.* **245**, 472–480 (1996).

30. Scheller, E. L. & Rosen, C. J. What's the matter with MAT? Marrow adipose tissue, metabolism, and skeletal health. *Ann. N. Y. Acad. Sci.* **1311**, 14–30 (2014).

31. Scheller, E. L. *et al.* Region-specific variation in the properties of skeletal adipocytes reveals regulated and constitutive marrow adipose tissues. *Nat. Commun.* **6**, 7808 (2015).

32. Kurabayashi, T. *et al.* Effects of a b 3 Adrenergic Receptor Agonist on Bone and Bone Marrow Adipocytes in the Tibia and Lumbar Spine of the Ovariectomized Rat. *Calcif. Tissue Int.* **68**, 248–254 (2001).

33. Burkhardt, R. *et al.* Changes in trabecular bone, hematopoiesis and bone marrow vessels in aplastic anemia, primary osteoporosis, and old age: a comparative histomorphometric study. *Bone* **8**, 157–164 (1987).

34. Siclari, V. A. *et al.* Mesenchymal progenitors residing close to the bone surface are functionally distinct from those in the central bone marrow. *Bone* **53**, 575–586 (2013).

35. Beresford, J. N., Bennett, J. H., Devlin, C., Leboy, P. S. & Owen, M. E. Evidence for an inverse relationship between the differentiation of adipocytic and osteogenic cells in rat marrow stromal cell cultures. *J. Cell Sci.* **102**, 341–351 (1992).

36. Meunier, P., Aaron, J., Edouard, C. & Vignon, G. Osteoporosis and the replacement of cell populations of the marrow by adipose tissue. A quantitative study of 84 iliac bone biopsies. *Clin. Orthop.* **80**, 147–154 (1971).

37. Patsch, J. M. *et al.* Bone marrow fat composition as a novel imaging biomarker in postmenopausal women with prevalent fragility fractures. *J. Bone Miner. Res.* **28**, 1721–1728 (2013).

38. Schwartz, A. V. Marrow fat and bone: review of clinical findings. *Bone Res.* **6**, 40 (2015).

39. Chatterjee, M. *et al.* A robust methodology for the quantitative assessment of the rat jawbone microstructure. *Int. J. Oral Sci.* **9**, 87–94 (2017).

40. Du, Z. *et al.* Estrogen deficiency associated bone loss in the maxilla: a methodology to quantify the changes in the maxillary intra-radicular alveolar bone in an ovariectomized rat osteoporosis model. *Tissue Eng. Part C Methods* 141015001219004 (2014). doi:10.1089/ten.TEC.2014.0268

41. Jiao, K. *et al.* Age- and sex-related changes of mandibular condylar cartilage and subchondral bone: A histomorphometric and micro-CT study in rats. *Arch. Oral Biol.* **55**, 155–163 (2010).

42. Buie, H. R., Campbell, G. M., Klinck, R. J., MacNeil, J. A. & Boyd, S. K. Automatic segmentation of cortical and trabecular compartments based on a dual threshold technique for in vivo micro-CT bone analysis. *Bone* **41**, 505–515 (2007).

43. Otsu, N. A Threshold Selection Method from Gray-Level Histograms. *IEEE Trans. Syst. Man Cybern.* **9**, 62–66 (1979).

44. Massart, D. L. *Handbook of chemometrics and qualimetrics. Part A Part A*. (Elsevier, 1997).

45. Johnston, B. D. & Ward, W. E. The Ovariectomized Rat as a Model for Studying Alveolar Bone Loss in Postmenopausal Women. *BioMed Res. Int.* **2015**, 1–12 (2015).

46. Ejiri, S. *et al.* Estrogen deficiency and its effect on the jaw bones. *J. Bone Miner. Metab.* **26**, 409–415 (2008).

47. Tanaka, M., Ejiri, S., Kohno, S. & Ozawa, H. Region-specific Bone Mass Changes in Rat Mandibular Condyle following Ovariectomy. *J. Dent. Res.* **79**, 1907–1913 (2000).

48. Tanaka, M., Toyooka, E., Kohno, S., Ozawa, H. & Ejiri, S. Long-term changes in trabecular structure of aged rat alveolar bone after ovariectomy. *Oral Surg. Oral Med. Oral Pathol. Oral Radiol. Endodontology* **95**, 495–502 (2003).

49. Yang, J., Pham, S. & Crabbe, D. Effects of oestrogen deficiency on rat mandibular and tibial microarchitecture. *Dentomaxillofacial Radiol.* **32**, 247–251 (2003).

50. Kribbs, P. J., Chesnut, C. H., Ott, S. M. & Kilcoyne, R. F. Relationships between mandibular and skeletal bone in an osteoporotic population. *J. Prosthet. Dent.* **62**, 703–707 (1989).

51. Wang, X. *et al.* Site-Specific Characteristics of Bone Marrow Mesenchymal Stromal Cells Modify the Effect of Aging on the Skeleton. *Rejuvenation Res.* **19**, 351–361 (2015).

52. Aghaloo, T. l. *et al.* Osteogenic Potential of Mandibular vs. Long-bone Marrow Stromal Cells. *J. Dent. Res.* **89**, 1293 (2010).

53. Chaichanasakul, T., Kang, B., Bezouglaia, O., Aghaloo, T. L. & Tetradis, S. Diverse Osteoclastogenesis of Bone Marrow From Mandible Versus Long Bone. *J. Periodontol.* **85**, 829–836 (2014).

54. Tokalov, S. V., Grüner, S., Schindler, S., Iagunov, A. S. & Abolmaali, M. B. and N. D. A Number of Bone Marrow Mesenchymal Stem Cells but Neither Phenotype Nor Differentiation Capacities Changes with Age of Rats. *Mol. Cells* **24**, 255–260 (2007).

55. Baron, R., Tross, R. & Vignery, A. Evidence of sequential remodeling in rat trabecular bone: Morphology, dynamic histomorphometry, and changes during skeletal maturation. *Anat. Rec.* **208**, 137–145 (1984).

599 56. Vignery, A. & Baron, R. Dynamic histomorphometry of alveolar bone remodeling in the adult
600 rat. *Anat. Rec.* **196**, 191–200 (1980).
601 57. Erben, R. G. Trabecular and endocortical bone surfaces in the rat: Modeling or remodeling?
602 *Anat. Rec.* **246**, 39–46 (1996).
603 58. Wronski, T. J., Lowry, P. L., Walsh, C. C. & Ignaszewski, L. A. Skeletal alterations in
604 ovariectomized rats. *Calcif. Tissue Int.* **37**, 324–328 (1985).
605 59. Wronski, T. J., Walsh, C. C. & Ignaszewski, L. A. Histologic evidence for osteopenia and
606 increased bone turnover in ovariectomized rats. *Bone* **7**, 119–123 (1986).
607 60. Mavropoulos, A., Kiliaridis, S., Bresin, A. & Ammann, P. Effect of different masticatory
608 functional and mechanical demands on the structural adaptation of the mandibular alveolar bone
609 in young growing rats. *Bone* **35**, 191–197 (2004).
610 61. Huja, S. S., Fernandez, S. A., Hill, K. J. & Li, Y. Remodeling dynamics in the Alveolar Process in
611 Skeletally Mature Dogs. *Anat. Rec. A. Discov. Mol. Cell. Evol. Biol.* **288**, 1243–1249 (2006).
612 62. Allen, M. R. The effects of bisphosphonates on jaw bone remodeling, tissue properties, and
613 extraction healing. *Odontology* **99**, 8–17 (2011).
614 63. Akintoye, S. O. *et al.* Skeletal site-specific characterization of orofacial and iliac crest human
615 bone marrow stromal cells in same individuals. *Bone* **38**, 758–768 (2006).
616 64. Jiang, J. M. Y., Sacco, S. M. & Ward, W. E. Ovariectomy-Induced Hyperphagia Does Not
617 Modulate Bone Mineral Density or Bone Strength in Rats. *J. Nutr.* **138**, 2106–2110 (2008).
618 65. Chappard, D. *et al.* Medullar fat influences texture analysis of trabecular microarchitecture
619 on X-ray radiographs. *Eur. J. Radiol.* **58**, 404–410 (2006).
620
621

ADDITIONAL FIGURES & LEGENDS

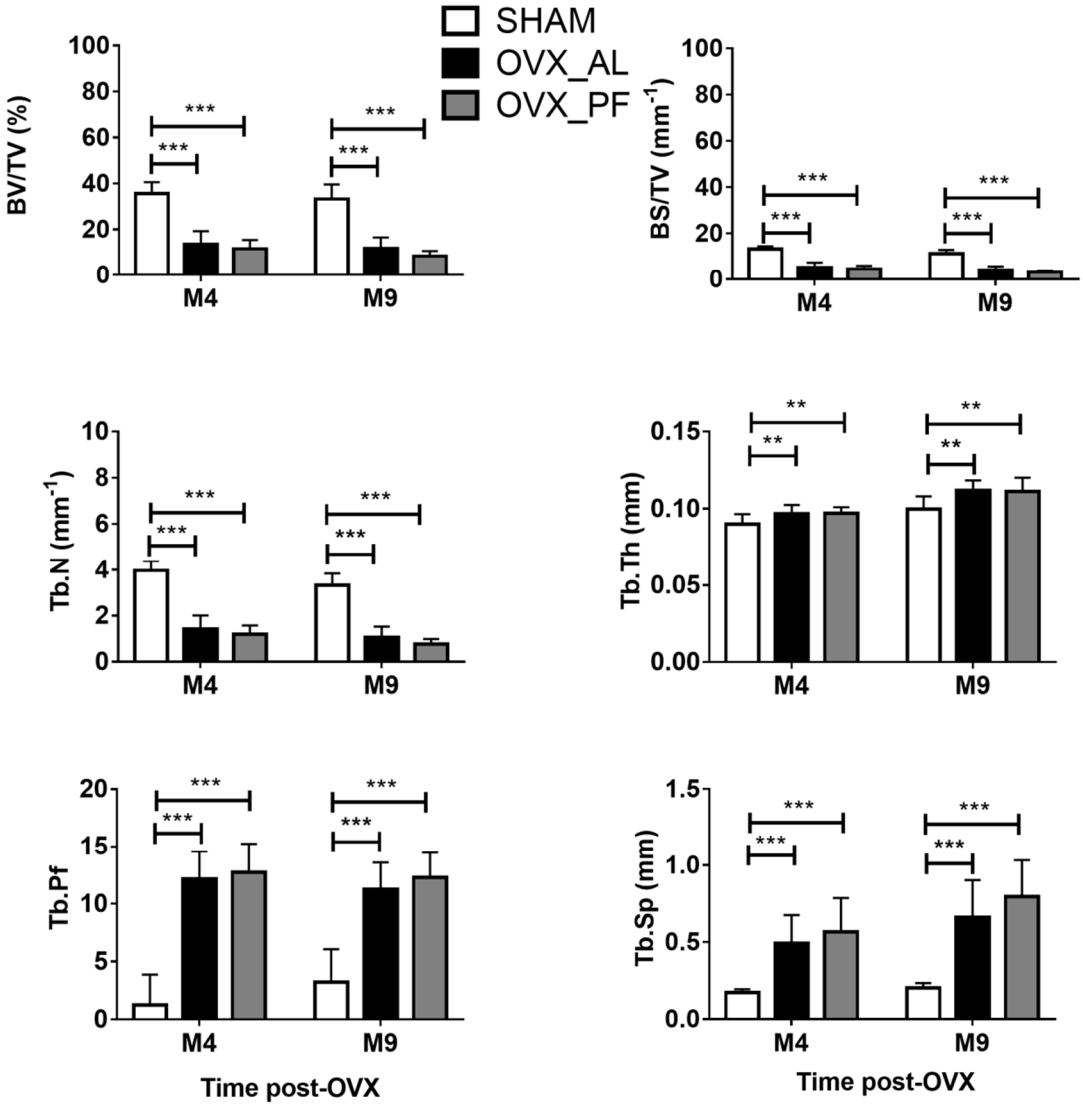

Figure 8 : OVX-related effect on trabecular bone microarchitecture respectively at M4 and M9 in the tibia. Values are means ± SD. Differences between groups are shown: **p<0.01, *** p<0.0001

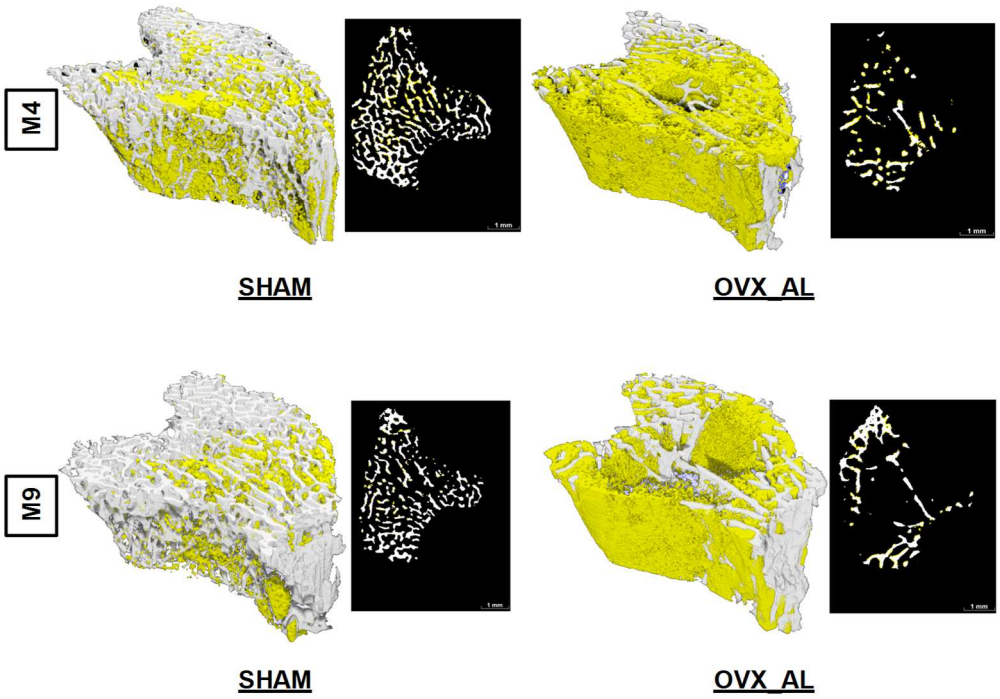

627

628 **Figure 9 : 3D micro-CT rendering of trabecular bone microarchitecture (white) and BMAT**
629 **(yellow) in the proximal metaphysis of the tibia at M4 (top) and M9 (bottom) in SHAM**
630 **groups (left) and OVX_AL (right). Each volume representation is associated with a 2D**
631 **transverse cross-section illustrating in 2D the BMAT in contact with the trabecular bone**
632 **surface.**

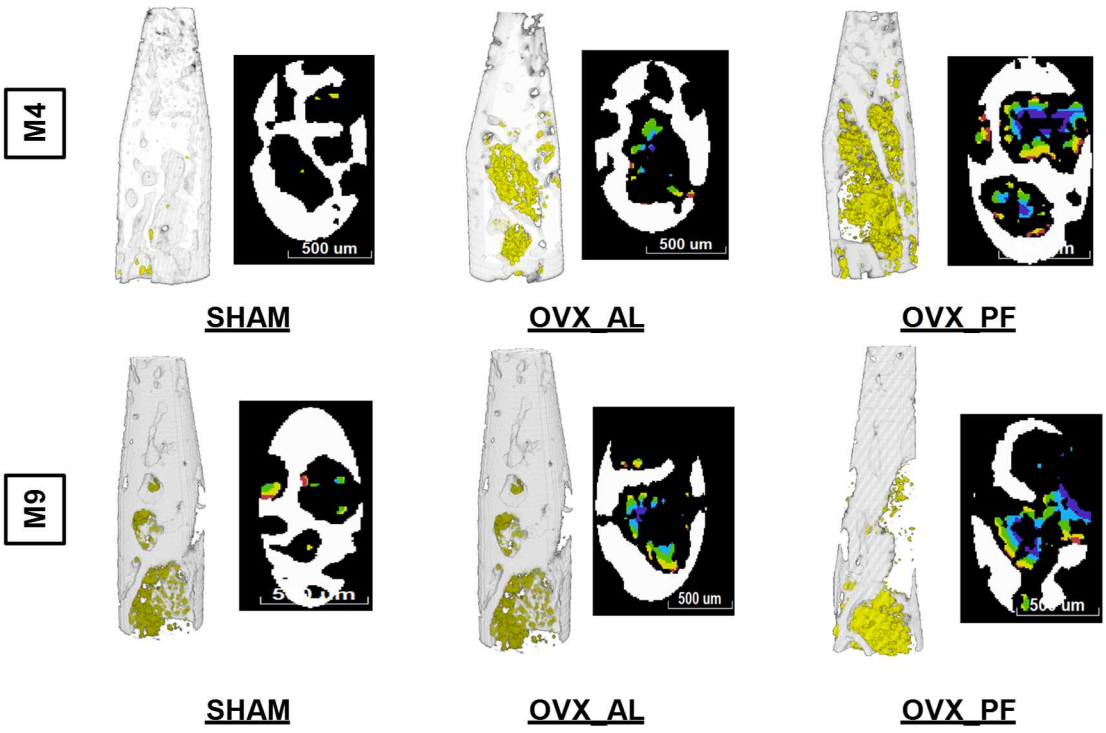

633

634 **Figure 10 : 3D micro-CT rendering of trabecular bone microarchitecture (white) and BMAT**
635 **(yellow) in the alveolar bone at M4 (top) and M9 (bottom) in SHAM (left) , OVX_AL**
636 **(middle) and OVX_PF groups (right). Each volume representation is associated with a 2D**
637 **transverse cross-section illustrating the distribution of BMAT in relation to the trabecular**
638 **bone surface (red: 0-20µm, yellow: 20-40µm, green: 40-60µm, blue: 60-80µm, purple: 80-**
639 **100µm)**

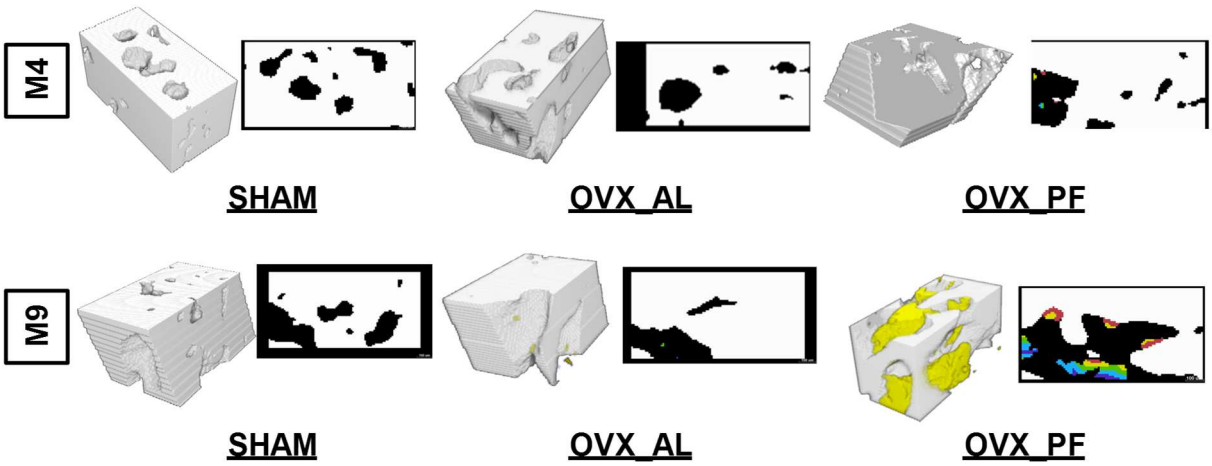

640

641 **Figure 11 : 3D micro-CT rendering of trabecular bone microarchitecture (white) and BMAT**
642 **(yellow) in the condyle at M4 (top) and M9 (bottom) in SHAM (left), OVX_AL (middle) and**
643 **OVX_PF groups (right). Each volume representation is associated with a 2D transverse**
644 **cross-section illustrating the BMAT distribution in relation to the condylar bone surface**
645 **(red: 0-20µm, yellow: 20-40µm, green: 40-60µm, blue: 60-80µm, purple: 80-100µm)**